Article

Angular-Ratiometric Plasmon-Resonance Based Light Scattering for Bioaffinity Sensing

Kadir Aslan, Patrick Holley, Lydia Davies, Joseph R. Lakowicz, and Chris D. Geddes

J. Am. Chem. Soc., **2005**, 127 (34), 12115-12121• DOI: 10.1021/ja052739k • Publication Date (Web): 04 August 2005

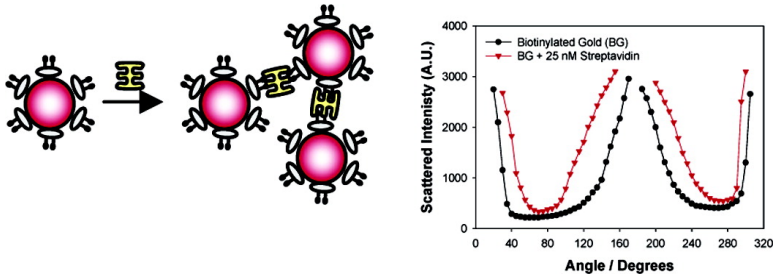

More About This Article

Additional resources and features associated with this article are available within the HTML version:

- Supporting Information
- Links to the 13 articles that cite this article, as of the time of this article download
- Access to high resolution figures
- Links to articles and content related to this article
- Copyright permission to reproduce figures and/or text from this article

View the Full Text HTML

J|A|C|S
ARTICLES
Published on Web 08/04/2005

Angular-Ratiometric Plasmon-Resonance Based Light Scattering for Bioaffinity Sensing

Kadir Aslan,[†] Patrick Holley,[†] Lydia Davies,[†] Joseph R. Lakowicz,[‡] and Chris D. Geddes*[,†,‡]

Contribution from the Institute of Fluorescence, Laboratory for Advanced Medical Plasmonics, Medical Biotechnology Center, University of Maryland Biotechnology Institute, 725 West Lombard Street, Baltimore, Maryland 21201, and Center for Fluorescence Spectroscopy, Medical Biotechnology Center, University of Maryland School of Medicine, 725 West Lombard Street, Baltimore, Maryland 21201

Received April 27, 2005; E-mail: geddes@umbi.umd.edu

Abstract: We describe an exciting opportunity for affinity biosensing using a ratiometric approach to the angular-dependent light scattering from bioactivated and subsequently aggregated noble metal colloids. This new model sensing platform utilizes the changes in particle scattering from very small colloids, which scatter light according to traditional Rayleigh theory, as compared to the changes in scattering observed by much larger colloidal aggregates, formed due to a bioaffinity reaction. These larger aggregates no longer scatter incident light in a $\mathrm{Cos}^2\,\theta$ dependence, as is the case for Rayleigh scattering, but instead scatter light in an increased forward direction as compared to the incident geometry. By subsequently taking the ratio of the scattered intensity at two angles, namely 90° and 140°, relative to the incident light, we can follow the association of biotinylated bovine serum albumin-coated 20 nm gold colloids, cross-linked by additions of streptavidin. This new model system can be potentially applied to many other nanoparticle assays and has many advantages over traditional fluorescence sensing and indeed light-scattering approaches. For example, a single nanoparticle can have the equivalent scattered intensity as 10^5 fluorescing fluorescein molecules substantially increasing detection; the angular distribution of scattered light from noble metal colloids is substantially easier to predict as compared to fluorescence; the scattered light is not quenched by biospecies; the ratiometric measurements described here are not dependent on colloid concentration as are other scattering techniques; and finally, the noble metal colloids are not prone to photodestruction, as is the case with organic fluorophores.

1. Introduction

Dynamic Light Scattering (DLS), also referred to as photon correlation spectroscopy,[1] is the most widely used technique today for studying colloidal systems.[2−5] It is a relatively fast technique which can provide absolute estimates of particle size and concentration for a wide variety of particles. However, the technique does have several limitations.[1] These include the low information content from the measured signal, the complexity of data analysis (this involves the numerical inversion of a Laplace Transform[1]) and the fact that both DLS and the other scattering techniques are not appropriate for very dilute solutions of particles.[2−5] Subsequently, this has been a limitation in sensing biospecies at nanomolar and even lower concentrations.

However, over the last several years the use of both gold and silver nanoparticles in biological assays has dramatically increased. This has been afforded by their very high molar absorption coefficients,[6,7] which has enabled their use in many absorption-based (of light) nanoparticle assays.[8−14] In addition to their high absorption cross-sections ($\epsilon = 1.68 \times 10^{10}$ M^{-1} cm^{-1} for a 30 nm Ag particle, 380 nm),[6] nanoparticles of gold and silver are also very efficient scatterers of light ($C_{scat} = 8 \times 10^{-12}$ cm^2 for a 30 nm Ag particle, 380 nm).[6] Indeed a noble metal colloid's extinction spectrum is composed of both an absorption and scattering component, which is contrary to how we think of a typical fluorophores extinction spectrum. Subsequently, light scattering by gold and silver nanoparticles can be detected at concentrations as low as 10^{-16} M.[6] In addition,

[†] Institute of Fluorescence.
[‡] Center for Fluorescence Spectroscopy.

(1) Bryant, G.; Thomas, J. C. *Langmuir* **1995**, *11*, 2480−2485.
(2) Dahneke, B. E. Ed. *Measurements of Suspended Particles by Quasi-Elastic Light Scattering*; Wiley-Interscience: New York, 1983.
(3) Chu, B. *Laser Light Scattering*, 2nd ed.; Academic Press: New York, 1991.
(4) Brown, W. Ed. *Dynamic Light Scattering: The Method and Some Applications*; Clarendon Press: Oxford, U.K., 1993.
(5) Finay, R. *Adv. Colloid Interface Sci.* **1994**, *52*, 79−143.
(6) Yguerabide, J.; Yguerabide, E. *Anal. Biochem.* **1998**, *262*, 137−156.
(7) Yguerabide, J.; Yguerabide, E. *Anal. Biochem.* **1998**, *262*, 157−176.
(8) Aslan, K.; Lakowicz, J. R.; Geddes, C. D. *Anal. Chem. Acta* **2004**, *517*, 139−144.
(9) Aslan, K.; Lakowicz, J. R.; Geddes, C. D. *Anal. Biochem.* **2004**, *330*, 145−155.
(10) Reynolds, R. A.; Mirkin, C. A.; Letsinger, R. L. *J. Am. Chem. Soc.* **2000**, *122*, 3795−3796.
(11) Elghanian, R.; Storhoff, J. J.; Mucic, R. C.; Letsinger, R. L.; Mirkin, C. A. *Science* **1997**, *277*, 1078−1081.
(12) Sastry, M.; Lala, N.; Patil, V.; Chavan, S. P.; Chittiboyina, A. G. *Langmuir* **1998,** *14*, 4138−4142.
(13) Cobbe, S.; Connolly, S.; Ryan, D.; Nagle, L.; Eritja, R.; Fitzmaurice, D. *J. Phys. Chem. B* **2003**, *107*, 470−477.
(14) Nath, N.; Chilkoti, A. *Anal. Chem.* **2002**, *74*, 504−509.

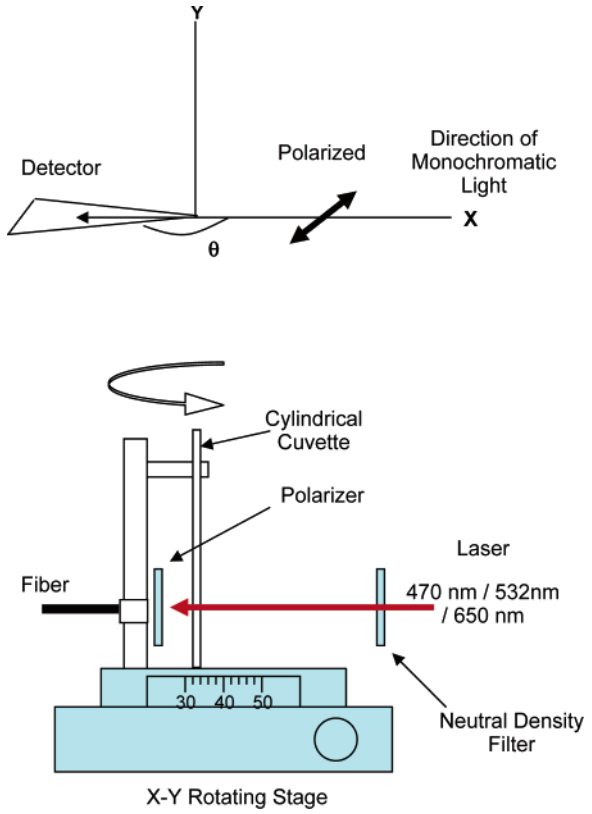

Figure 1. Coordinate system used to describe the geometrical arrangement of the illumination (Perp. excitation) and detection systems (top) and the apparatus used for measuring the angular dependence of colloidal scatter (bottom).

it is well-known that the light dependent scattering properties of a nanoparticle depend on their size, shape, composition, and the refractive index of the suspending medium.[6] However, one property that has been ill explored for biosensing applications is the angular dependence (spatial distribution) of plasmon scatter,[15] as we describe herein.

When a metallic nanoparticle is exposed to an electromagnetic wave, the electrons in the metal (plasmons) oscillate at the same frequency as the incident wave.[6] Subsequently, the oscillating electrons radiate electromagnetic radiation with the same frequency as the oscillating electrons. It is this reradiation of light at the same incident wavelength, which is often referred to as plasmon scatter.[6]

The scattering of light by very small subwavelength sized particles is well described by Rayleigh theory.[16] For incident light traveling along the *x*-axis, Figure 1 (top), and polarized in the *z*-axis, the intensity of light scattered, I_{scatt}, in the direction θ by a homogeneous spherical particle with radius a, that is much smaller than the wavelength, λ, of the incident beam, is given by the Rayleigh expression;[6,16]

$$I_{scatt} = \frac{16\pi^4 a^6 n_{med}{}^4 I_0}{r^2\lambda^4} \left| \frac{m^2-1}{m^2+2} \right|^2 \mathrm{Cos}^2\,\vartheta \qquad (1)$$

where I_0 is the incident intensity of monochromatic light, n_{med} is the refractive index surrounding the particle, m is the refractive index of the bulk particle material (both functions of the incident wavelength), and r is the distance between the particle and where the scattered light is detected. From Figure 1 (top) the polarization vector lies in the *xz*-plane, and this scattered light is 100% polarized. Interestingly from Figure 1 and eq 1, the scattered light intensity is highest at the observation angles $\theta = 0°$ and 180°, is zero at $\theta = 90°$ and 270°, the intensity being proportional to $\mathrm{Cos}^2\,\theta$. This spatial or angular distribution of plasmon scatter is characteristic of an electric dipole emitter.[6] Equation 1 is ideally suited for single particle scattering or for particle suspensions where the particles are sufficiently spaced so that interpretable perturbations and multiple scatterings are insignificant. For very dilute samples of multiple particles, where the absorbance of the incident wavelength is less than 0.005 [6] then the intensity of the scattered light can be obtained by multiplying the single particle scattering intensity expressions by the particle concentration, p, (particles/cm^3). The intensity is therefore proportional to the nanoparticle concentration, and the dilute solution has the same angular distribution of scatter, and degree of polarization, as an individual "Rayleigh particle".[6]

However, for larger particles, where the size of the nanoparticle is approximately greater than $^1/_{20}$ the wavelength of light, or for Rayleigh sized particles in close proximity to one another, the scattering properties no longer obey Rayleigh theory but indeed can be described by Mie's theory.[17] The angular dependence of plasmonic scatter subsequently changes from the $\mathrm{Cos}^2\,\theta$ dependence described by eq 1 (Rayleigh limit) to a much more complex spatial distribution of scatter, where the degree of forward scatter (i.e., 180° in our geometry, Figure 1) increases with particle size (Mie limit).[17]

It is informative to briefly describe why the scattering from larger particles is no longer described by Rayleigh theory. It was previously mentioned that when a small particle is exposed to an electromagnetic field, whose wavelength is much larger than the diameter of the particle, then the electrons in the nanoparticle all sense the same phase of the incident wave, and therefore all scatter light with the same phase. In essence, the whole particle behaves as a large oscillating dipole moment, a function of the collective electron oscillations (plasmons). However, for much larger particles, then the electrons on the particles can experience different phases and therefore can oscillate with different phases. This inherently leads to interference of the light which is scattered by the electrons from different parts of the particles. Subsequently, both the magnitude and angular distribution of the scattered light deviate from that expected of a normal oscillating electric dipole. While beyond the scope of this text, Mie theory for light scattering from large particles can be considered as light radiating from oscillating electric dipoles, as well as magnetic dipoles, quadruples, and other higher order magnetic multipoles.[17] Scattered light by Mie theory is well-known to be described by the following equation[17]

$$I_{scatt} = \frac{2\pi}{k^2} \sum_{n=1}^{\infty} (2n+1)(|a_n|^2 + |b_n|^2) \qquad (2)$$

where $k = 2\pi n_{med}/\lambda$. One can envision the different terms in the sum as corresponding to different electric and magnetic multipoles and n is the term index. The term with $n = 1$ corresponds to the electric dipole. The coefficients a_n and b_n

(15) Souza, G. R.; Miller, J. H. *J. Am. Chem. Soc.* **2001**, *123*, 6734−6735.
(16) Kerker, M. *The Scattering of Light and Other Electromagnetic Radiation*; Academic Press: New York, 1969.
(17) Mie, G. *Ann. Phys.* **1908**, *25*, 377−445.

are defined in terms of the Bessel and Ricatti functions and in general are complex numbers depending on whether the refractive index of the particle is real or complex.[6] When the particle is much smaller than the wavelength of light, the most important expression in the Mie equation becomes that of the electric dipole, and then the Mie equation reduces back to the Rayleigh expression.

To demonstrate the utility of our new sensing approach, we first demonstrate the angular dependence of laser-light scatter from different sized gold colloids. These colloids range in size from 20 to 200 nm, where the differences in their angular distribution of scatter serve to confirm and support our observations for a bioaffinity solution based assay, where small nanoparticles aggregate into much larger structures using proteins.

The angular distribution (spatial distribution) of scatter from different sized colloids is known to be markedly different[6] but has never been utilized for sensing. For small particles whose diameters are less than $^1/_{20}$ the wavelength of light, then this is described well by Rayleigh theory,[6,16] whereas Mie theory[17] describes the scattering from the much larger structures. As we will show, the $\mathrm{Cos}^2\ \theta$ dependence of scatter from small unaggregated particles in the Rayleigh limit is no longer a valid description of the scattering distribution for much larger, aggregated particles. In this regard, we have been careful to choose unaggreagted colloids (monomers) whose scatter can initially be well described by Rayleigh theory but, after protein induced aggregation, now resides in the Mie limit for scattering. As mentioned, the initial choice of nanoparticle size is paramount for the biosensing platform described in this paper. Rayleigh theory applies quite strictly to particles for which the radius $a \ll < \lambda/(2\pi n_{med}m)$. For silver colloids and the wavelengths discussed here, m is usually not greater than 4.[6] For $m = 4$, $\lambda = 532$ and 650 nm and $n_{\mathrm{med}} = 1.33$, this expression yields particles with radii of 15.9 and 19.4 nm, respectively. According to Yguerabide,[6] particles up to about 40 nm are still considered to be in the Rayleigh limit. Subsequently for this work, we have chosen to use 20 nm gold colloids, which can be purchased monodispersed from Ted Pella, CA.

In addition to "breaking" the $\mathrm{Cos}^2\ \theta$ angular dependence of Rayleigh scatter by protein aggregation of the nanoparticles as an approach to sensing, we have also been able to ratio the scattered intensities at different angles, so that our measurements become independent of light fluctuations, background light, and most importantly nanoparticle concentration, which is not the case with other light scattering techniques.[1−5] This subsequently allows us to quantitatively measure the concentration of protein in our model system, or potentially any species that induces nanoparticle aggregation. We therefore envisage that this angular-ratiometric plasmon-resonance based light scattering approach for bioaffinity sensing will serve as a model system which could readily be applied to the many other nanoparticle assays which have been developed.[8−14]

2. Results and Discussion

To demonstrate our sensing approach, whereby the angular dependence of plasmonic scatter changes upon colloidal aggregation induced by a bioaffinity reaction, we first studied the scattering behavior of uncoated gold colloid suspensions. Figure 2 shows the normalized absorption spectra of different sized gold colloids in citrate buffer. We can clearly see the plasmon absorption band at 520 nm for 20 nm colloids, shifting red, as well as broadening as a function of size. This is consistent with other reports.[14,18] Subsequently, for the angular scattering dependences discussed in this paper, we used monochromatic laser light at 470, 532, and 650 nm, which is similar to the plasmon absorption maxima of the colloids.[14,18]

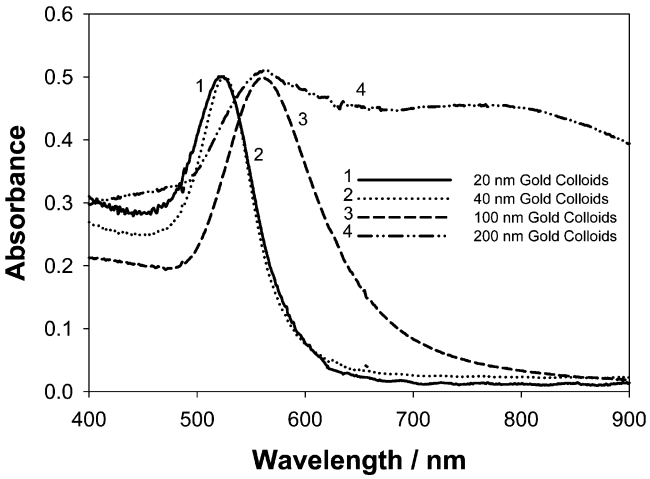

Figure 2. Normalized absorption spectra of different sized gold colloids.

For bioaffinity sensing based on the angular dependence of plasmon scatter, it is important to understand the concentration dependence of the colloids on the scattering spatial distribution. Figure 3 shows the angular scattering profiles for different concentrations of 20 nm colloids using 532 nm monochromatic laser light. As predicted by eq 1, the $\mathrm{Cos}^2\ \theta$ dependence on scattering can clearly be seen in these dilute samples. At angles approaching 0°, 180°, and 360°, the scattering is the most pronounced, minimums in the scattering occurring at 90° and 270°, respectively. As expected the two sets of scattering curves in Figure 3 (top) are mirror images of each other and simply reflect the 0°−180° and 180°−360° regions, as the fiber optic detector is rotated around the samples, cf. Figure 1 (bottom). Approaching 0°, 180°, and 360°, the detector is rapidly saturated and hence the intensity values at 0°, 180°, and 360° were not measurable. In fact, the dynamic range of scattering presented in Figure 3 (top) is a compromise between the laser power used and being able to detect both the minimum and maximum scattering intensities. Subsequently, for the data shown in this paper, we typically record scattering intensities from 40° to 160° and 200° to 320°.

Rayleigh theory for the scattering of light by dilute solutions of small colloids predicts that the scattering intensity at a given angle increases as a function of colloid concentration. This can be clearly seen in Figure 3 (top insert), which is simply the enlarged 80°−100° region. However, by taking the ratio of any two intensities, in our case we have chosen 90° and 140°, then the scattered intensities become independent of the colloid concentration. In addition, these angular ratiometric measurements are independent of excitation (light fluctuations) or detector drifts as well as background room light, notable features for biosensing. It should be noted that our data were not taken simultaneously at all angles, but in fact the detector fiber was

(18) Collier, C. P.; Vossmeyer, T.; Heath, J. R. *Annu. Rev. Phys. Chem.* **1998**, *49*, 371−404.

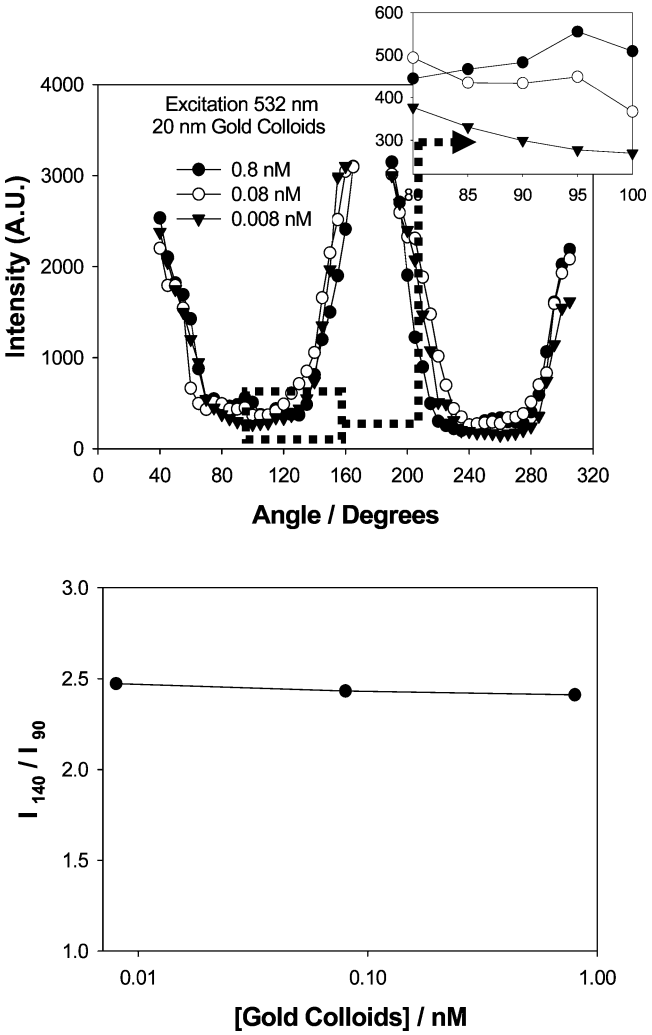

Figure 3. Angular dependent scattering of 20 nm colloids using 532 nm laser light as a function of colloid concentration (top), enlarged 80°−100° region (top insert) and the I_{140}/I_{90} intensity ratio Vs colloid concentration (bottom).

swept around the sample to demonstrate the $\mathrm{Cos}^2\,\theta$ dependence of plasmon scatter and the utility of our sensing approach. However, one can envisage that, for actual real-world bioaffinity sensing, two fibers could simultaneously measure plasmon scatter at any two unique angles, thus potentially making the measurements independent of experimental artifacts.

Figure 3 (bottom) indeed demonstrates this sensing strategy and shows an angular-ratiometric plot of intensities recorded at 140° and 90° as a function of 20 nm gold colloid concentration. The almost linearity of the plot shows that the concentration of the colloids does not change the spatial distribution of the scatter, which is a most important consideration for sensing applications. In addition, the concentration range studied typically reflects that used in colloidal plasmon absorption type biosensing assays[19−21] and was the reason for its choice. In this regard, our choice of colloid concentration for sensing is deemed on the limit of where the concentration of the colloids has no or little effect on the sensing data.

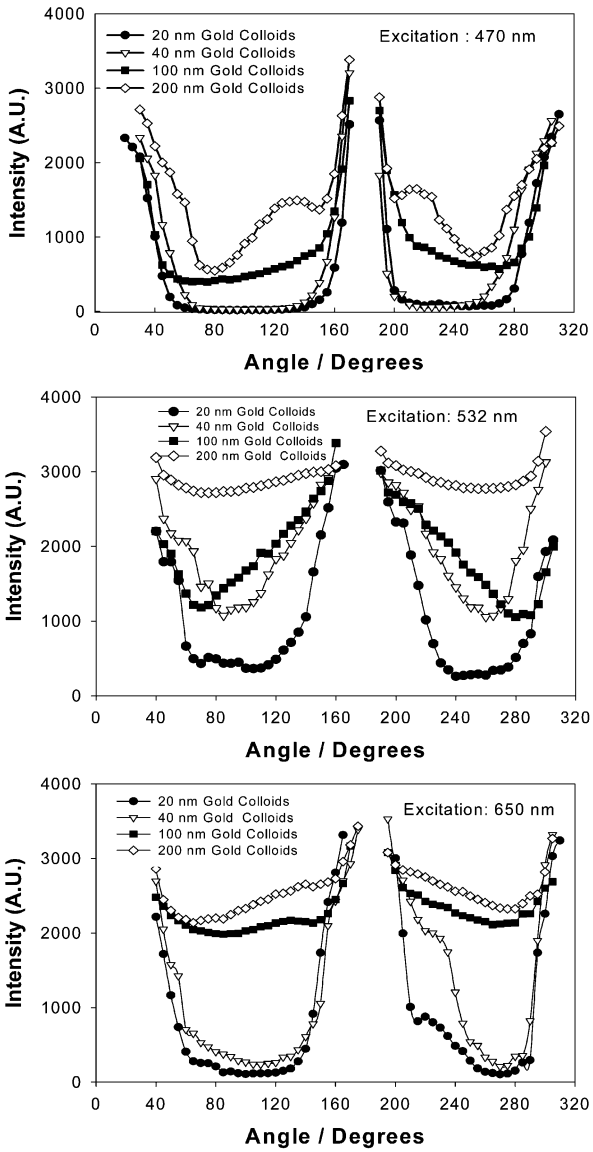

Figure 4. Angular dependent scattering from 0.8 nM different sized gold colloids using 470 nm (top), 532 nm (middle), and 650 nm (bottom) laser light.

Figure 4 shows the angular dependent scattering from 0.8 nM different sized gold colloids using 470, 532, and 650 nm laser light, top to bottom, respectively. There are two main features to these plots: first, the colloidal size dependence of scattering at a given incident wavelength, and second, the differences in scattering distributions for a given colloid size using different incident wavelengths.

At a given incident wavelength, all the plots show a size dependence on scattering distribution, Figure 4. These results show that the scattering from 20 nm colloids typically follows a $\mathrm{Cos}^2\,\theta$ dependence as depicted by Rayleigh theory, i.e., eq 1. As the colloidal size increases, the angular scattering profiles become much more complex and are no longer described by the Rayleigh expression but can indeed be described by Mie's theory.[17] In Mie's theory, the degree of forward scatter increases as the particle size increases.[17] From Figure 4 (middle), we can clearly see this, as the width of the scattering spectrum at 180° increases as a function of colloidal size. In our system, 180° is the angle of forward scatter, cf. Figure 1. It should be noted

(19) Roll, D.; Malicka, J.; Gryczynski, I.; Gryczynski, Z.; Lakowicz, J. R. *Anal. Chem.* **2003**, *75*, 3108−3113.
(20) Mayes, A. G.; Blyth, J.; Millington, R. B.; Lowe, C. R. *Anal. Chem.* **2002**, *74*, 3649−3657.
(21) Kim, Y.; Johnson, R. C.; Hupp, J. T. *Nano Lett.* **2001**, *1* (4), 165−167.

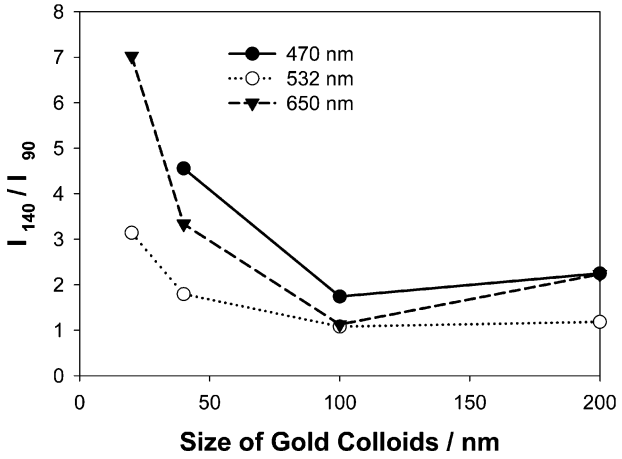

Figure 5. Intensity ratio at 140° and 90° Vs colloid size for three different incident wavelengths.

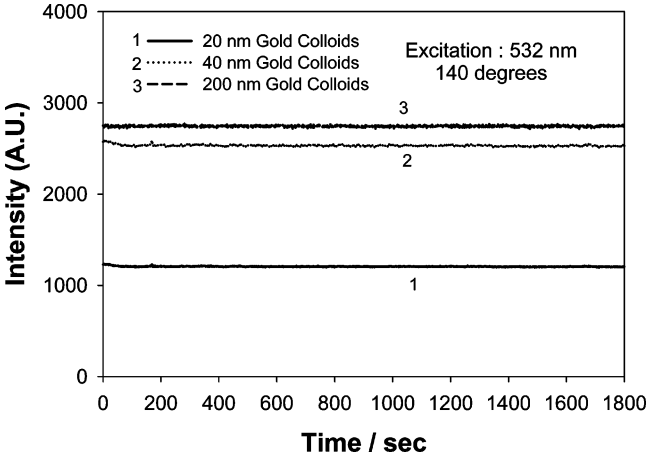

Figure 6. 532 nm, 140° scattered intensity for different sized colloids as a function of time.

that in our experimental system we found the data not to be totally symmetrical about the 180° axis. This we explain as due to the imperfect positioning of the laser foci in the center of sample chamber and also the nonisotropic scattering from walls of the chamber itself.

Subsequently, by taking the ratio of the scattered intensities at 90° and 140° as a function of gold colloid size, Figure 5, we can clearly see how the size distribution of scatter is changing. For small colloids, the I_{140}/I_{90} ratio is quite large, in the range 3−7, as the scattering follows a $\mathrm{Cos}^2\,\theta$ dependence. However, for much larger colloids the discrete $\mathrm{Cos}^2\,\theta$ scattering distributions are lost; the scattering no longer follows a $\mathrm{Cos}^2\theta$ dependence, and the ratio becomes close to unity, Figure 5.

For our bioaffinity sensing scheme, briefly discussed in the Introduction and discussed in more detail later, we have carefully chosen our initial gold colloid size to be in the Rayleigh limit, i.e., 20 nm. Upon protein-induced aggregation of the colloids, the scattering distributions become increasingly more complex as a function of protein addition, the scattering no longer following a $\mathrm{Cos}^2\,\theta$ dependence. Similar to the unmodified colloids, the I_{140}/I_{90} ratio changes and can subsequently be correlated with protein concentration, or indeed any analyte or biospecies which can induced colloidal aggregation. Importantly, the dynamic range of the sensing strategy manifests itself in being able to aggregate particles which initially scatter in the Rayleigh limit, into the Mie limit after aggregation, cf. the range shown in Figure 5.

From Figures 4 and 5 we can also see that the scattering distribution and therefore the I_{140}/I_{90} ratio for a given colloid size change with incident wavelength, respectively. Unlike the colloidal size dependence for a fixed incident wavelength, these trends are much more complex to interpret and are due to both the absorption and scattering components of a colloid's extinction spectrum,[6] in addition to the position of the plasmon absorption maximum.[6,14,18] For the sensing scheme discussed later in this paper we have chosen to use both 532 and 650 nm incident wavelengths. This is because 20 nm colloids have a plasmon absorption maxima at ∼520 nm[14−18] and the potential applications of this technology to biological sensing and the respective need to alleviate biological autofluorescence by using longer incident wavelengths.[22]

(22) Lakowicz, J. R. *Principles of Fluorescence Spectroscopy*; Kluwer/Academic Plenum Publishers: New York, 1997.

Finally, to investigate both the photostability of the colloids, as well as to ascertain whether the colloids would settle out of solution as a function of time, we monitored the scattering intensity as a function of time using 532 nm incident light measured at 140°, Figure 6. For all colloid sizes and also the BSA-biotin colloids described later, we found that the intensity remained constant over the 30 min measurement period. This was particularly encouraging and demonstrates that both the colloids do not settle from solution during measurements and that the laser powers employed in this study (several mW) do not alter the shape of the colloids, as has been reported by some authors, but for higher incident laser powers.[23] From Figure 6 we can see that the colloids are photostable, more so than traditional fluorophores, which are prone to photodegradation,[22] their scattering distributions not changing as a function of time.

2.1 Bioaffinity Assay Monitored by Angular-Ratiometric Plasmon-Resonance Based Light-Scattering. To demonstrate the utility of our approach and its broader applicability to biological sensing, we chose a model protein system, Figure 7.

Biotinylated bovine-serum albumin-coated 20 nm colloids (BSA-colloids) can be readily prepared, which cluster by the addition of the tetravalent protein streptavidin.[19] The hypothesis of our approach was that one would expect to see changes in the scattering distribution of associated colloids, in a similar manner as that observed for the scattering dependence of increasingly larger sized colloids as shown in Figures 4 and 5. Indeed, many workers have reported the shifts in absorption spectra as a function of aggregation for sensing, but changes in the angular distribution of the scattering portion of the extinction spectrum for sensing, during association, has been ill explored to date. In addition, our model system was chosen as the association of biotin and streptavidin is very strong,[19] eliminating the possibility of back disassociation reactions to complicate our model system's kinetics.

Figure 8 (top) shows the normalized absorption spectra of BSA-colloids as a function of streptavidin addition. The absorption spectra were taken after completion of the aggregation, which was typically 45 min for each sample. Figure 8 (bottom) shows the time dependent change in absorption at 600 nm for a 15 nM streptavidin addition. After 2000 s, we can see that the reaction is essentially >90% complete.

(23) Millard, M.; Huang, P.; Brus, L. *Nano Lett.* **2003**, *3*, 1611−1615.

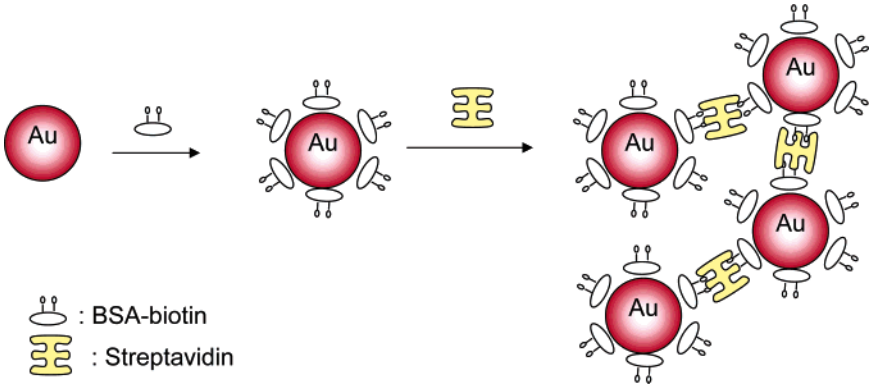

Figure 7. Model system (BSA-Biotin colloids cross-linked by steptavidin) to demonstrate the utility of angular-ratiometric plasmon-resonance based light scattering for affinity biosensing.

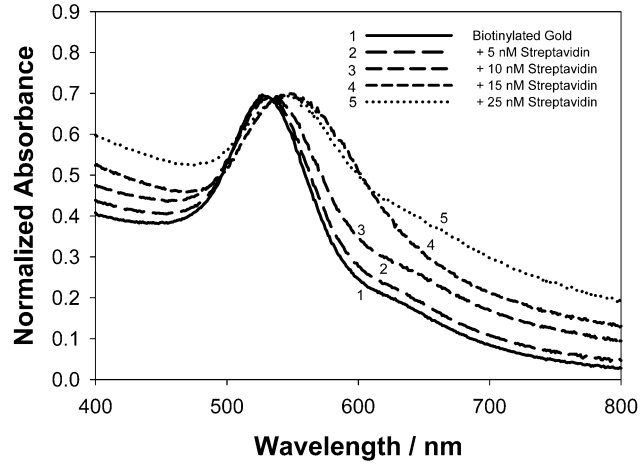

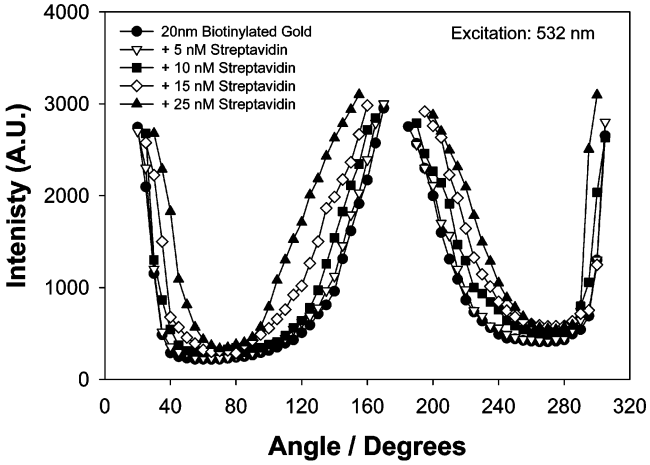

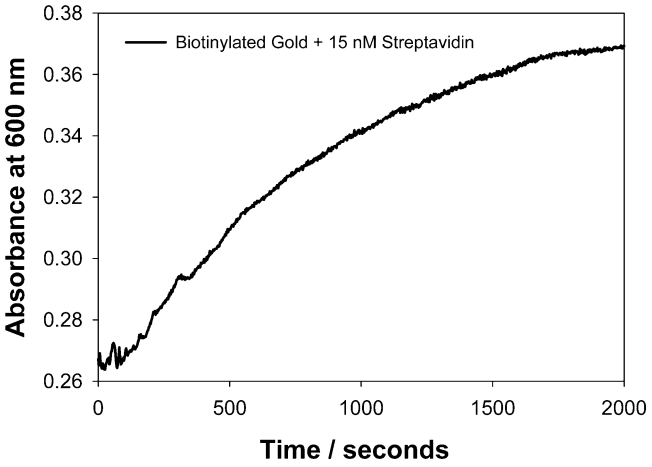

Figure 8. Changes in absorption spectra of BSA-biotin colloids cross-linked by streptavidin (top) and the time dependent change in absorption at 600 nm for a 15 nM streptavidin addition (bottom).

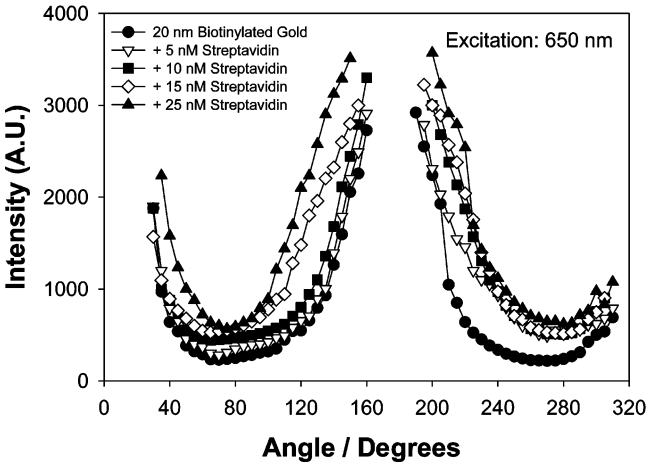

Figure 9. Angular dependent scattering from 20 nm BSA-biotin colloids cross-linked by streptavidin (45 min incubation) from 532 nm (top) and 650 nm laser light (bottom).

Identical concentration and compositions of BSA-colloids were subsequently incubated with different concentrations of streptavidin for 45 min, and the angular scattering profiles then taken using both 532 (Figure 9, top) and 650 nm (Figure 9, bottom) incident light, in an analogous manner to the virgin colloids described earlier. From Figure 9 we can clearly see that the streptavidin induced association reaction changes the angular scattering profile from a relatively simple $\mathrm{Cos}^2\ \theta$ dependence in the absence of streptavidin to one much more complex, with a higher degree of forward scatter. These changes are consistent with a change in scattering from Rayleigh like particles to particles in the Mie limit as depicted by eqs 1 and 2. Importantly, by taking the I_{140}/I_{90} intensity ratio, we are able to follow the BSA-colloid association reaction as a function of streptavidin addition, Figure 10. Using this model system, we have been able to observe a notable change in the I_{140}/I_{90} intensity ratio using 532 and 650 nm incident light. While we have chosen a relatively simple model system to demonstrate

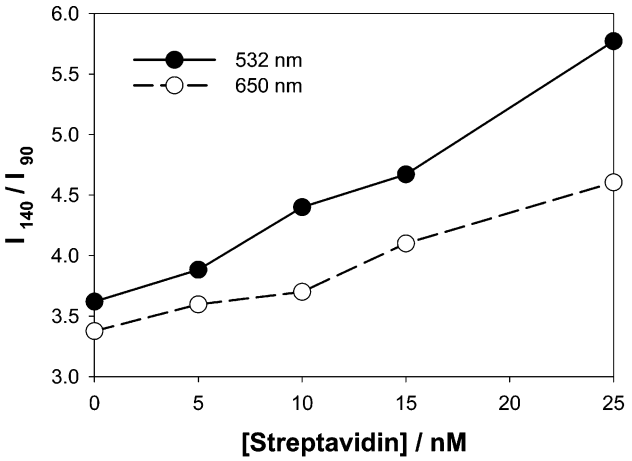

Figure 10. I_{140}/I_{90} scattered intensity ratio from aggregated BSA-biotin colloids for both 532 and 650 nm laser light as a function of streptavidin concentration (45 min incubation time).

our approach, this approach could be applied to monitor the many other nanoparticle biological association/disassociation reactions.

2.2. Advantages of this Sensing Platform for Bioaffinity Sensing. In this paper we have demonstrated a cheap and simplistic approach to bioaffinity sensing. Our approach has many notable advantages in terms of instrumentation, using nanoparticles as compared to fluorophores for sensing, as well as advantages over other scattering-based techniques. Most notably:

(1) In most nanoparticle assays to date, one typically measures the bioinduced change in plasmon absorption.[8−14] This involves moderately complex instrumentation,[22] in that a subtractive light measurement is undertaken (absorption measurement) which is usually scanned over many wavelengths. However, for our angular-ratiometric plasmon-resonance based light scattering approach, a bioaffinity reaction can be followed by simply measuring and taking the ratio of the scattered light intensity from a laser line at two unique angles. This is a notable step forward in the simplification and cost of the sensing instrumentation.

(2) By taking the ratio of the scattered intensity at two angles, the sensing approach is independent of nanoparticle concentration, cf. Figure 5, which is not the case for DLS and other scattering techniques.[1−5]

(3) The spatial distribution of scatter from colloids is much simpler to predict than fluorescence from fluorophores.[6]

(4) Fluorophores are prone to photodestruction over time by intense illumination intensities, such as those used in microscopy.[22] Colloids are not prone to photodestruction under the same conditions.

(5) The lifetime of plasmon scatter is usually less than 1 ps, whereas fluorescence lifetimes are usually on a nanosecond time scale. Subsequently, plasmon light scatter is not prone to quenching by biospecies, unlike many fluorophores.[6,22]

3. Conclusions

In this paper we have demonstrated a model sensing platform that could be applied to many other nanoparticle based assays.

20 nm gold colloids which scatter 532 and 650 nm laser light in an angular $\mathrm{Cos}^2\,\theta$ dependence readily change their spatial scattering distribution upon aggregation. The resultant aggregates no longer have a spatial distribution of scatter that can be described by the Rayleigh expression. By subsequently taking the ratio of the scattered intensities at two angles, we are readily able to quantitatively follow the bioinduced aggregation of the nanoparticles, independently of the nanoparticle concentration, a notable feature for biosensing. The dynamic range for sensing has been optimized by carefully choosing unaggregated particles that initially scatter light according to the Rayleigh expression, but after bio-induced aggregation, scatter light with a different spatial (angular) distribution, i.e., $\neq \mathrm{Cos}^2\theta$.

4. Materials and Methods

4.1. Materials. Colloidal gold dispersions (20, 40, 100, and 200 nm) were purchased from Ted Pella. Sodium phosphate monobasic, phosphate buffered saline (PBS), streptavidin, biotinamidocaproyl labeled bovine serum albumin (biotinylated BSA), and standard glass NMR tubes (5 mm, series 300) were purchased from Sigma-Aldrich. All chemicals were used as received.

4.2. Methods. 4.2.1. Preparation of Biotinylated BSA-Coated 20 nm Gold Colloids. The surface modification of 20 nm gold colloids was performed using an adapted version of the procedure found in the literature.[19] In this regard, 5 mL of the gold colloid solution were mixed with 0.05 mL of aqueous solution of biotinylated BSA (1.44 mg/mI), and this mixture was incubated at room temperature for 2 h. The gold colloid/biotinylated BSA mixture was then centrifuged in an Eppendorf centrifuge tube equipped with a 100 000 MW cutoff filter for 10 min, using an Eppendorf microcentrifuge at 8000*g*, to separate the biotinylated BSA-coated gold colloids from the excess biotinylated BSA. The supernatant was carefully removed, and the pellet containing the biotinylated gold colloids was resuspended in 10 mM sodium phosphate buffer (pH 7). This was subsequently used in the aggregation assays.

4.2.2. Aggregation Assay Using Biotinylated Gold Colloids and Streptavidin. The model aggregation assay, used to demonstrate the utility of our approach, was performed by mixing biotinylated gold colloids (20 nm) with increasing concentrations of streptavidin in a quartz cuvette. In this regard, a 1000 nM stock solution of streptavidin (prepared in PBS based on the specifications provided by manufacturer, E1% at 282 nm = 31.0) was added to 0.5 mL of biotinylated gold colloid samples and incubated at room temperature for 30 min. To achieve the desired final streptavidin concentrations, predetermined volumes of streptavidin stock solution were used. The degree of aggregation was measured by recording the absorption spectrum of each sample (as with all other absorption measurements), using a Varian Cary 50 spectrophotometer.

4.3.3. Angle-Dependent Scattering Measurements of Gold Colloids and the Bioaffinity Aggregation Assay. The angle-dependent scattering from gold colloids of various sizes and those used in the aggregation assay were measured using an X−Y rotating stage (Edmund Optics), that was modified to hold a cylindrical cuvette (a thin walled NMR tube), with a fiber optic mount (Figure 1, bottom). The gold colloids were illuminated with three different polarized laser sources: 470, 532, and 650 nm, a neutral density filter being used to adjust the laser intensity. The angle-dependent polarized scattered light from the gold colloids was collected through a dichroic sheet polarizer (Edmund optics) into a 600 micron broad wavelength fiber that was connected to an Ocean Optics HD2000 spectrofluorometer.

The photostability of 20, 40, and 200 nm gold colloids, under constant illumination with a 532 nm laser, was measured by simply observing the scattered intensity at 140° for 30 min.

Acknowledgment. This work was supported by the NIH GM070929 and the National Center for Research Resources, RR008119. Partial salary support to C.D.G. and J.R.L. from UMBI is also acknowledged.

JA052739K